ISBN: 978-84-693-6437-6

Hydrodynamic Models for GaN-Based HEMTs

S. Vitanov, V. Palankovski, and S. Selberherr*
Advanced Material and Device Analysis Group
*Institute for Microelectronics, Technische Universität Wien
A-1040, Vienna, Austria
Email: {vitanov|palankovski|selberherr}@iue.tuwien.ac.at

***Abstract*— For the development of next-generation GaN-based high electron mobility transistors, reliable software tools for DC and AC simulation are required. A hydrodynamic approach must be used, as the drift diffusion models fail to deliver accurate results for such structures. We propose two different hydrodynamic mobility models which account for the peculiarities of the GaN material system. The models are implemented in our simulator Minimos-NT and carefully calibrated. A device from a recent transistor generation is measured and simulated using the calibrated setup. A good accuracy for all relevant characteristics is achieved.**

I. Introduction

Models which account for the specific physics in a given semiconductor material are crucial for device modeling. While for Silicon there exist well-established models, the GaN system still poses certain challenges. The major one is caused by the negative differential electron mobility (NDM) predicted by Monte Carlo (MC) simulations e.g. [1], [2]. Several works provide direct evidences of this effect: a peak velocity at 191 kV/cm in lightly doped material was first reported in [3], however later studies observed a velocity saturation and adjacent decrease at around 225 kV/cm [4]. While the latter measurement was in normal plane, measurements in basal plane yielded saturation velocity at 180 kV/cm in *n*-type GaN and at 140 kV/cm in AlGaN/GaN heterostructures [5]. Indirect evidence of NDM in GaN, such as transferred-electron effects in Gunn diodes also exist [6]. Nevertheless, a definite examination of the problem is still pending since not only the saturation velocity reported by different groups are contradictive (depending largely on the material and orientation), but also there is still no agreement on the reason for the NDM (intervalley transfer or nonparabolic effect). Therefore, a model for GaN has to be capable of describing NDM effects, while providing some straightforward approach to fine-tuning the velocity characteristics at high electric fields.

Several groups have proposed various models and model parameter sets for the simulation of GaN-based devices. Farahmand *et al.* provide a low-field model which accounts for temperature and the ionized impurity concentrations, as well as a high-field model, based on Monte Carlo simulation results [7]. Another low-field model, valid in a large temperature and concentration range is proposed by Mnatsakanov *et al.* [8]. A highly parameterized field-dependent model based on an extensive data pool is developed by Schwierz [9]. Turin *et al.* propose another high-field model which delivers excellent agreement with the results from MC simulations [10]. All those models are suited only for the drift-diffusion transport model. However, the latter is not able to deliver accurate results for sub-micron devices [11], therefore a hydrodynamic (HD) transport model is essential. In this work we propose two models specific to the hydrodynamic simulation of GaN-based devices. Our models are calibrated against MC simulation results and experimental data and implemented in the two-dimensional device simulator MINIMOS-NT [12], which has proven to be a suitable tool for the analysis of heterostructure devices [13],[14]. Using the calibrated setup we simulate a device from a recent generation of AlGaN/GaN HEMTs. Very good accuracy for the DC and AC characteristics in comparison to measurement results is achieved.

A. Low-Field Mobility

Since AlGaN/GaN HEMTs are unipolar devices, the hole concentration is very low and does not influence the device characteristics [15]. Thus, the presented models are tailored to the electron transport, while for the hole transport conventional models are applied.

The low-field mobility is modeled by an expression similar to that proposed by Caughey and Thomas [14], [16]:

$$\mu^{\mathrm{LI}} = \mu^{\min} + \frac{\mu^{\mathrm{L}} - \mu^{\min}}{1 + (C_{\mathrm{I}}/C^{\mathrm{ref}})^{\alpha}}.$$

C_{I} denotes the concentration of ionized impurities, μ^{L} is the mobility in undoped material, $\mu^{\min}$ is the mobility in highly doped material, limited by impurity scattering. In order to model the temperature dependence the mobilities are additionally parameterized using power laws:

$$\alpha = \alpha_{300}\left(\frac{T_{\mathrm{L}}}{300\ \mathrm{K}}\right)^{\gamma_0},$$
$$\mu^{\mathrm{L}} = \mu^{\mathrm{L}}_{300}\left(\frac{T_{\mathrm{L}}}{300\ \mathrm{K}}\right)^{\gamma_1},\ \mu^{\min} = \mu^{\min}_{300}\left(\frac{T_{\mathrm{L}}}{300\ \mathrm{K}}\right)^{\gamma_2}.$$

The maximum (μ^{L}) and minimum ($\mu^{\min}$) mobility and the parameters, which describe the mobility decrease with rising

TABLE I
Low-Field Mobility Parameters

μ^{L}_{300}	$\mu^{\min}_{300}$	C^{ref}_{300}	α_{300}	γ_0	γ_1	γ_2
1600 $\mathrm{cm^2/Vs}$	100 $\mathrm{cm^2/Vs}$	$3\times10^{17}\mathrm{cm^{-3}}$	0.7	0.065	-1.5	-0.2

ISBN: 978-84-693-6437-6

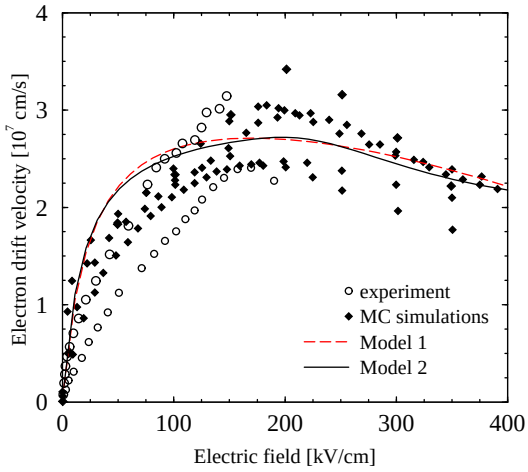

Fig. 1. Electron drift velocity versus electric field: simulations with different mobility models compared to MC simulation results and experimental data.

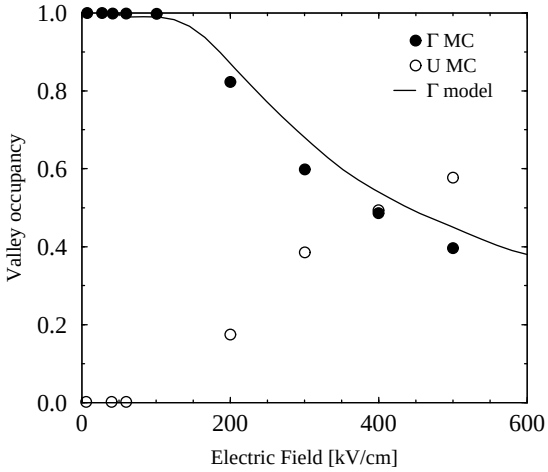

Fig. 2. Valley occupancy as a function of the electric field.

impurity concentration (C_{300}^{ref} and α_{300}) are calibrated against an extensive analysis of available MC simulations results and experimental data. Our model assumes the high mobility consistent with the defect-free substrates of the simulated devices. A profound discussion on the choice of the parameters describing the temperature dependence (γ_1, γ_2) based on experimental data from measurements at elevated ambient temperature can be found in [17]. The values used for the low field-mobility in the simulations are listed in Table I.

B. High-Field Mobility

The models proposed for the high-field mobility are based on the mobility expression of the form [18]:

$$\mu(E) = \frac{\mu^{\mathrm{LI}}}{\xi + \left((1-\xi)^{\beta} + \left(\frac{\mu^{\mathrm{LI}} \cdot E}{v_{\mathrm{sat}}} \right)^{\beta} \right)^{1/\beta}}. \tag{1}$$

μ^{LI} is the low-field electron mobility as calculated previously, v_{sat} is the electron saturation velocity, E is the electric field. The same expression with different values for ξ and β was used by [19].

In order to obtain a consistent hydrodynamic mobility expression, the local energy balance equation:

$$E^2 \cdot \mu = \frac{3 \cdot \mathrm{k_B} \cdot \Delta T_{\mathrm{n}}}{2 \cdot q \cdot \tau_{\epsilon}} \tag{2}$$

is solved for $E(T_{\mathrm{n}})$, which is then inserted into (1). This is performed with ξ=1/2 for both models, and with β=2 for the first model, and β=1 for the second model, respectively. T_{n} is the electron temperature and τ_{ϵ} is the energy relaxation time.

a) Model 1: The expression obtained with the chosen values for ξ and β is identical with the one proposed by Hänsch *et al.* [20]. In order to account for NDM effects it is modified by introducing two parameters (γ_1 and γ_2):

$$\begin{aligned} \mu(T_{\mathrm{n}}) &= \frac{\mu^{\mathrm{LI}} \cdot (T_{\mathrm{n}}/T_{\mathrm{L}})^{\gamma_3}}{\left(1 + \alpha^{1/\gamma_4} \cdot (T_{\mathrm{n}} - T_{\mathrm{L}})^{1/\gamma_4}\right)^{\gamma_4}} \\ \alpha &= \frac{3 \cdot \mathrm{k_B} \cdot \mu^{\mathrm{LI}}}{2 \cdot \mathrm{q} \cdot \tau_{\epsilon} \cdot (v_{\mathrm{f}})^2}. \end{aligned}$$

In the standard Hänsch model v_{f} corresponds to the saturation velocity v_{sat} (as in (1)). However, due to the powered temperature term $(T_{\mathrm{n}}/T_{\mathrm{L}})^{\gamma_3}$ in the numerator the velocity is steadily decreasing at high-fields. Hence, v_{f} does not describe the saturation velocity as a physical quantity, although it does affect the high-field transport characteristics. τ_{ϵ} is the electron and lattice temperature dependent energy relaxation time (a quadratic expression is used). The parameter γ_4 has a more pronounced effect at low fields, while γ_3 influences primarily the high-field mobility, though their impact cannot be isolated to a specific field region. The conventional Hänsch model corresponds to the parameter set γ_3=0, γ_4=1, however, in order to approximate the simulation and experimental data, a set with $\gamma_3 = -0.3$ and $\gamma_4 = 2.4$ is chosen (Fig. 1).

b) Model 2: Inserting (2) into (1) with ξ=1/2 and β=2 gives the following expression for the high-field mobility:

$$\begin{aligned} \mu_{\mathrm{v}}(T_{\mathrm{n}}) &= \frac{2 \cdot \mu_{\mathrm{v}}^{\mathrm{LI}}}{2 + \alpha_{\mathrm{v}} + \sqrt{\alpha_{\mathrm{v}} \cdot (4 + \alpha_{\mathrm{v}})}}, \mathrm{v} = \Gamma, \mathrm{U} \\ \alpha_{\mathrm{v}} &= \frac{3 \cdot \mathrm{k_B} \cdot \mu_{\mathrm{v}}^{\mathrm{LI}} \cdot (T_{\mathrm{n}} - T_{\mathrm{L}})}{2 \cdot \mathrm{q} \cdot \tau_{\mathrm{v}} \cdot (v_{\mathrm{f,v}})^2}. \end{aligned}$$

In order to approximate the intervalley transfer at high fields, two sets of $\mu_{\mathrm{v}}(T_{\mathrm{n}})$ are used. One describes the mobility $\mu_{\Gamma}(T_{\mathrm{n}})$ in the lower valley and one in the higher ($\mu_{\mathrm{U}}(T_{\mathrm{n}})$). In Model 2 too, v_{f} does not denote the saturation velocity. A weighted mean is built:

$$\mu(T_{\mathrm{n}}) = \frac{\mu_{\Gamma}(T_{\mathrm{n}}) + \mu_{\mathrm{U}}(T_{\mathrm{n}}) \cdot P_{\mathrm{HD}}(T_{\mathrm{n}})}{1 + P_{\mathrm{HD}}(T_{\mathrm{n}})} \tag{3}$$

ISBN: 978-84-693-6437-6

TABLE II
HIGH-FIELD MOBILITY PARAMETERS

μ_Γ μ^{LI}	μ_U μ^{LI}	$v_{\mathrm{f},\Gamma}$ [cm/s]	$v_{\mathrm{f},U}$ [cm/s]	τ_U τ_ϵ	τ_Γ τ_ϵ	ΔE_C [eV]	m^*_Γ m_0	m^*_U m_0
1.0	0.1	3.0×10^7	1.0×10^7	1.0	8.0	1.4	0.2	0.3

$P_{\mathrm{HD}}(T_\mathrm{n})$ is the valley occupancy [21]:

$$P_{\mathrm{HD}}(T_\mathrm{n}) = 6 \cdot \left(\frac{m^*_\mathrm{U}}{m^*_\Gamma}\right)^{3/2} \cdot \exp\left(-\frac{\Delta E_\mathrm{C}}{\mathrm{k_B} \cdot T_\mathrm{n}}\right),$$

m^*_Γ and m^*_U are the electron masses in the Γ and U valleys respectively, ΔE_C is the difference in the conduction bands. Fig. 2 compares the valley occupancy as a function of the electric field as calculated in the model and MC simulation. Since all MC simulations and experiments, on which we rely to calibrate the low-field mobility, were performed at low electric fields, we set μ_Γ=μ_{LI} as calculated by the low-field mobility model. Using a down-scaled mobility ($\mu_\mathrm{U} = 0.1\times\mu_{\mathrm{LI}}$ supported by MC data) and velocity parameter (v_f) in the higher band results in a decrease of the electron velocity at higher fields. The parameters for this model are summarized in Table II.

The two valley approach delivers a good approximation to the MC simulation results, but also to Model 1 (Fig. 1). It is a carefully chosen trade-off between a match the MC simulation results on the one hand, and calculation complexity and convergence behavior at the other hand.

While the models deliver consistent results, the two approaches expose some differences. Model 1 is close to already established models, and offers a straightforward calibration with only two auxiliary parameters (within a narrow value range). Model 2 is more complex, however it allows for a more flexible calibration. The parameters are derived from physical quantities.

The models are to be used for sub-micron devices. However, for large devices a drift-diffusion model is sufficient, while requiring a lower computational effort. Based on Model 2 a corresponding DD model can easily be synthesized. From (1) and ξ=1/2 and β=1 (the same set as in Model 2) again two sets of $\mu_\mathrm{v}(E)$ are calculated. The weighted mean is built corresponding to (3), but with an occupancy $\mathrm{P_{DD}}(E)$ as following:

$$P_{\mathrm{DD}}(E) = 6 \cdot \left(\frac{m^*_\mathrm{U}}{m^*_\Gamma}\right)^{3/2} \cdot \exp\left(-\frac{\Delta E_\mathrm{C}}{\mathrm{k_B} \cdot T_\mathrm{L} \cdot \left(1 + \frac{E}{E_0}\right)}\right).$$

All of the proposed models are suitable for TCAD implementation.

II. DEVICE DESCRIPTION

The AlGaN/GaN HEMT technology is based on multi-wafer metal oxide chemical vapor deposition (MOCVD) growth on 3-inch semi-insulating SiC substrates. The gate is e-beam defined. Device isolation is achieved by mesa isolation. An $\mathrm{Al_{0.22}Ga_{0.78}N}$/GaN heterointerface is grown on top of a thick insulating GaN buffer. All layers are unintentionally doped. We assume a metal diffusion of the metal source and drain contacts reaching into the channel. The positive charge (introduced by polarization effects) at the channel/barrier interface is compensated by a commensurate negative surface charge at the barrier/cap interface. Using the methodology as in [22] a theoretical value 1.2×10^{13} cm^{-2} for the $\mathrm{Al_{0.22}Ga_{0.78}N}$/GaN interface is calculated. However, in the real device several effects such as dislocations and surface states reduce the total sheet charge density. Thus, a lower value of 0.94×10^{13} cm^{-2} is used in the simulations, adapted in order to achieve a 2DEG density similar to the one extracted from Hall measurements. The barrier/cap and cap/passivation charge densities equal -0.25×10^{13} cm^{-2} and -0.4×10^{13} cm^{-2} respectively.

The device has a T-shaped gate with $\mathrm{l_g}$=0.25 μm and a gate width $\mathrm{W_g}$=2×50 μm (taken as 1×100 μm in the simulations). Contact resistance is 0.2 Ωmm.

Fig. 3 compares the measured transfer characteristics at $\mathrm{V_{DS}}$=7 V with simulations. The results achieved with Model 1

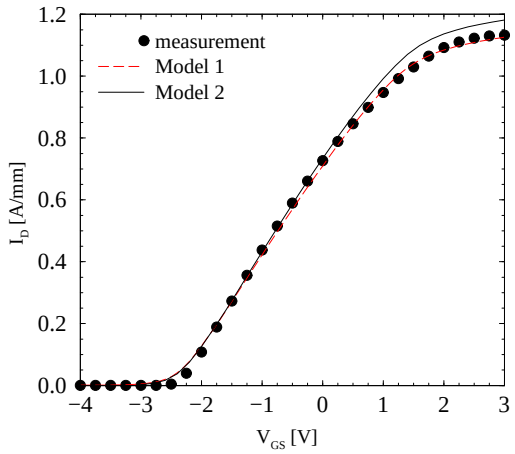

Fig. 3. Comparison of measured transfer characteristics and simulations.

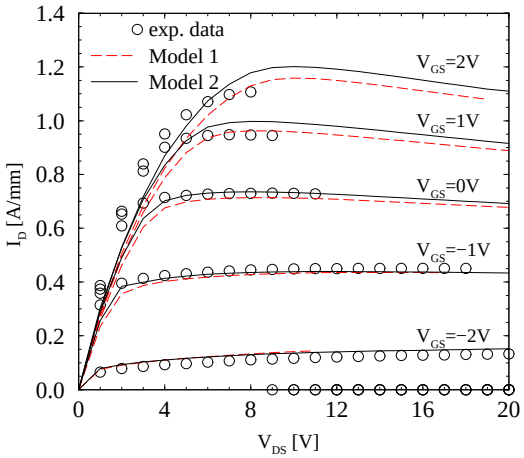

Fig. 4. Comparison of measured output characteristics and simulations.

ISBN: 978-84-693-6437-6

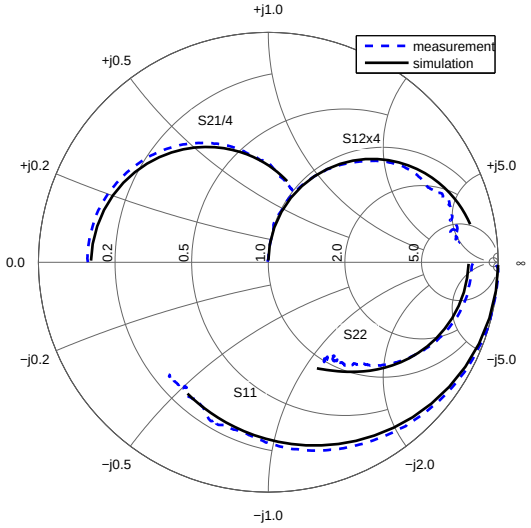

Fig. 5. Simulated S-parameters compared to measured data.

match slightly better, however the model delivers a lower current at low V_{DS} than measured (Fig. 4). One possible reason is a higher electron velocity at lower fields in the real device, due to low dislocation scattering effects.

AC simulations are performed to compare the calculated and experimental figures of merit e.g. cut-off and maximum frequency. In order to account for the parasitics introduced by the measurement equipment, the intrinsic parameters obtained in the simulation are transformed using a standard two-port pad parasitic equivalent circuit. Both models provide a very good agreement for the cut-off frequency with the experiment.

Fig. 5 compares the measured and simulated (using Model 2) extrinsic S-parameters at V_{GS}=-1.5 V and V_{DS}=7 V. An excellent agreement is achieved for all parameters in the frequency range 100 MHz−26 GHz.

III. Conclusion

We propose mobility models accounting for the specifics of electron transport in the GaN material system. They are implemented in a device simulator and simulations of a recent HEMT generation are conducted. The results are compared against experimental data and show excellent agreement. The presented TCAD methodology allows the design of next-generation GaN HEMTs through predictive simulations with a good accuracy at reasonable computational cost.

Acknowledgment

Support by the Austrian Science Funds FWF and BMWK, START Project No.Y247-N13 is acknowledged. The authors would like to thank S. Maroldt and R. Quay, IAF Freiburg, Germany for providing the experimental data.

References

[1] U. Bhapkar and M. Shur, “Monte Carlo calculation of velocity-field characteristics of wurtzite GaN,” *J.Appl.Phys.*, vol. 82, pp. 1649–1655, Aug. 1997.

[2] K. Brennan, E. Bellotti, M. Farahmand, H.-E. Nilsson, P. Ruden, and Y. Zhang, “Monte Carlo simulation of noncubic symmetry semiconducting materials and devices,” *IEEE Trans.Electron Devices*, vol. 47, no. 10, pp. 1882–1890, Oct. 2000.

[3] Z. Huang, R. Goldberg, J. Chen, Y. Zheng, D. Mott, and P. Shu, “Direct observation of transferred-electron effect in gan,” *Appl.Phys.Lett.*, vol. 67, no. 19, pp. 2825–2826, Nov. 1995.

[4] M. Wraback, H. Shen, J. Carrano, C. Collins, J. Campbell, R. Dupuis, M. Schurman, and I. Ferguson, “Time-resolved electroabsorption measurement of the transient electron velocity overshoot in GaN,” *Appl.Phys.Lett.*, vol. 79, no. 9, pp. 1303–1305, Aug. 2001.

[5] J. Barker, D. Ferry, D. Koleske, and R. Shul, “Bulk gan and algan/gan heterostructure drift velocity measurements and comparison to theoretical models,” *J.Appl.Phys.*, vol. 97, no. 6, p. 063705(5), June 2005.

[6] O. Yilmazoglu, K. Mutamba, D. Pavlidis, and T. Karaduman, “First observation of bias oscillations in gan gunn diodes on gan substrate,” *IEEE Trans.Electron Devices*, vol. 55, no. 6, pp. 1563–1567, June 2008.

[7] M. Farahmand, C. Garetto, E. Bellotti, K. F. Brennan, M. Goano, E. Ghillino, G. Ghione, J. Albrecht, and P. Ruden, “Monte Carlo simulation of electron transport in the III-Nitride wurtzite phase materials system: Binaries and ternaries,” *IEEE Trans.Electron Devices*, vol. 48, no. 3, pp. 535–542, Mar. 2001.

[8] T. Mnatsakanov, M. Levinshtein, L. Pomortseva, S. Yurkov, G. Simin, and M. Khan, “Carrier mobility model for GaN,” *Solid-State Electron.*, vol. 47, no. 1, pp. 111–115, Jan. 2003.

[9] F. Schwierz, “An electron mobility model for wurtzite GaN,” *Solid-State Electron.*, vol. 49, no. 6, pp. 889–895, Jun. 2005.

[10] V. O. Turin, “A modified transferred-electron high-field mobility model for GaN devices simulation,” *Solid-State Electron.*, vol. 49, no. 10, pp. 1678–1682, Oct. 2005.

[11] E. Faraclas and A. Anwar, “AlGaN/GaN HEMTs: Experiment and simulation of DC characteristics,” *Solid-State Electron.*, vol. 50, no. 6, pp. 1051–1056, June 2006.

[12] T. Binder, J. Cervenka, K. Dragosits, A. Gehring, T. Grasser, M. Gritsch, R. Klima, M. Knaipp, H. Kosina, R. Mlekus, V. Palankovski, M. Rottinger, R. Rodriguez-Torres, G. Schrom, S. Selberherr, M. Stockinger, and S. Wagner, *MINIMOS-NT Device and Circuit Simulator, User’s Guide, Release 2.0*, Institut für Mikroelektronik, Technische Universität Wien, 2002, http://www.iue.tuwien.ac.at/software/minimos-nt.

[13] V. Palankovski, R. Quay, and S. Selberherr, “Industrial application of heterostructure device simulation,” *IEEE J.Solid-State Circuits*, vol. 36, no. 9, pp. 1365–1370, Sep. 2001.

[14] V. Palankovski and R. Quay, *Analysis and Simulation of Heterostructure Devices*. Wien, New York: Springer, 2004.

[15] T. Simlinger, H. Brech, T. Grave, and S. Selberherr, “Simulation of submicron double-heterojunction high electron mobility transistors with MINIMOS-NT,” *IEEE Trans.Electron Devices*, vol. 44, no. 5, pp. 700–707, May 1997.

[16] D. Caughey and R. Thomas, “Carrier mobilities in silicon empirically related to doping and field,” *Proc.IEEE*, vol. 55, no. 12, pp. 2192–2193, Dec. 1967.

[17] S. Vitanov, V. Palankovski, S. Maroldt, and R. Quay, “High-temperature modeling of AlGaN/GaN HEMTs,” *Solid-State Electron.*, vol. In Press, pp. –, 2010.

[18] T. Grasser, H. Kosina, and S. Selberherr, “Consistent comparison of drift-diffusion and hydro-dynamic device simulations,” in *Proc. Simulation of Semiconductor Processes and Devices*, Kyoto, Japan, Sept. 1999, pp. 151–154.

[19] W. Hänsch and M. Miura-Mattausch, “The hot-electron problem in small semiconductor devices,” *J.Appl.Phys.*, vol. 60, no. 2, pp. 650–656, July 1986.

[20] W. Hänsch, M. Orlowski, and W. Weber, “The hot-electron problem in submicron MOSFET,” in *18th European Solid State Device Research Conference - ESSDERC 88*, ser. Journal de Physique, J.-P. Nougier and D. Gasquet, Eds., vol. 49, no. 9-C4. Les Ulis Cedex, France: les éditions de physique, 1988, pp. 597–606.

[21] S. Sze, *Physics of Semiconductor Devices*, 2nd ed. New York: Wiley, 1981.

[22] O. Ambacher, B. Foutz, J. Smart, J. Shealy, N. Weimann, K. Chu, M. Murphy, A. Sierakowski, W. Schaff, L. Eastman, R. Dimitrov, A. Mitchell, and M. Stutzmann, “Two-dimensional electron gases induced by spontaneous and piezoelectric polarization in undoped and doped AlGaN/GaN heterostructures,” *J.Appl.Phys.*, vol. 87, no. 1, pp. 334–344, Jan. 2000.